

Chapter 2

Preparation and Characterization of Colloidal Crystals for Synchrotron and Free Electron Laser X-ray Studies

Abstract In this chapter we describe the preparation and characterization of colloidal crystals for dedicated synchrotron and free-electron laser X-ray studies. The crystals were prepared via sedimentation and convective assembly followed by modifications for their application in the experiments. We illustrate two examples of the X-ray experiments, including the pump-probe experiments on the dynamics of laser heating of the colloidal particles on the crystal structure and structure melting around the glass transition temperature.

2.1 Introduction

Colloidal crystals and their internal structure have been the focus of many investigations because of their possible application as functional nanomaterials, for instance as photonic crystals [1–3]. The presence of defects in the crystal structure influences the functional properties of the colloidal crystal and therefore it is important to fully characterize both the crystal and defect structures in detail. Furthermore, investigations of the optical colloidal crystal properties, e.g. response of the photonic structure to strong optical fields, are important for technical feasibility of the crystals as photonic devices.

The improvement of 3rd generation X-ray sources has led to the development of novel X-ray techniques, such as hard and soft X-ray microscopy [4–6] as well as coherent X-ray diffraction imaging (CXDI) [7]. These methods can be applied to reveal the internal structure of the colloidal crystals [8]. In addition, the colloidal crystals are challenging model systems to test the CXDI data analysis, which involves complex iterative phase retrieval methods to reconstruct the real space image [9–11].

While the novel X-ray diffraction techniques offer new insights, they also demand stringent requirements for the sample preparation. In this chapter we describe the preparation of colloidal crystals from polystyrene and silica spheres via sedimentation and convective assembly that were used for different types of X-ray

studies. The aspects of preparation are discussed in detail and the obtained structures are characterized using microscopy techniques. The outline of this chapter is as follows. First, we discuss the experimental details of the preparation. Next, the optimal conditions to fabricate large scale single colloidal crystals via the vertical deposition method are discussed and the crystals characterized. This is followed by a discussion on the preparation and difficulties to obtain $\sim 5 \mu\text{m}$ colloidal crystal grains on a carbon fiber tip, which is needed to meet the sample requirements for a CXDI experiment. Finally, the results of two X-ray diffraction studies performed of these samples are briefly discussed.

2.2 Experimental

2.2.1 Colloidal Spheres

Several different colloidal sphere dispersions were used, with an average radius in the range of $R = 50\text{--}300 \text{ nm}$ and composed of either polystyrene or silica. The polystyrene particles were prepared by emulsifier-free emulsion polymerization of styrene using potassium persulfate as an initiator and are therefore charge stabilized by sulfate groups on their surface. The silica particles were prepared via the Stöber synthesis and were coated with 3-methacryloxypropyl trimethoxysilane (TPM) [12] or stearyl [13]. The size, radius R , and standard deviation, σ , of the particles was determined with transmission electron microscopy (TEM, Philips TECNAI10 or 12). For all particles used in this chapter the properties are listed in Table 2.1.

Table 2.1 Particle properties of all colloidal spheres and type of experiment they were employed in

Particle	Material	R (nm)	σ (%)	Experiment
PS1	Polystyrene	208	2.1	VD
PS2	Polystyrene	82	2.7	VD
PS3	Polystyrene	193	2.1	VD
CPS1	Crosslinked (3 %) polystyrene	97	4	VD
PS-R-B1271 ^a	Polystyrene	180	2.3	VD
BVR-I3	Crosslinked (3 %) polystyrene	136	4	VD
DB239 ^b	Silica-TPM	100	–	Sed
DB275 ^b	Silica-TPM	118	6	Sed, VD
DB284 ^b	Silica-Stearyl	116	–	Sed
DB359 ^b	Silica-Stearyl (<i>fluorescently labeled</i>)	110	–	Sed
DB360 ^b	Silica-TPM	246	3.2	Sed, VD

^aCommercial product obtained from microParticles GmbH, Germany

^bParticles obtained from “Deeltjesbank” at Van ’t Hoff Laboratory

2.2.2 Colloidal Crystal Preparation

Colloidal crystal films were prepared on different substrates via the vertical deposition method. Polystyrene and silica spheres were dispersed in water, ethanol or water/ethanol mixtures. For each vertical deposition setup, particle type and size the experimental conditions, including particle concentration, solvent, evaporation temperature and substrate inclination, were optimized. A typical vertical deposition experiment consisted of the preparation of a series of 0.1, 0.2, 0.5, 1 and 2 vol% polystyrene dispersions in water by diluting a desired amount of the stock dispersion with water to a total volume of 5 mL. The dispersion was placed into a scintillation vial of 20 mL and a glass substrates were placed into the dispersions at a desired angle. The solvent was evaporated by drying in an oven at 55 °C for ~48 h. The time needed for full evaporation of the 5 mL depends mostly on the solvent choice.

Glass substrates of various sizes were cut from glass slides of 24 × 50 mm (Menzel Gläser #1) to their desired size. The glass substrates were cleaned by soaking in a solution of 7.5 wt% potassium hydroxide (Merck, p.a.) in a mixture of ethanol (Merchachem, 100 %) and water (from a Millipore System) for the duration of 16 h, on some occasions only 1 h was employed.

Sedimentary colloidal crystals were only prepared of the silica particles because these can be dispersed in low density and volatile solvents, such as cyclohexane, ethanol and toluene. Non-crosslinked polystyrene particles will dissolve in most apolar solvents and their density difference with water is very low, $\Delta\rho = 0.05 \text{ g/cm}^3$, which makes their sedimentation a very slow process. The high density difference between the Stöber silica and the solvents, $\Delta\rho \approx 1 \text{ g/cm}^3$, is favorable for sedimentation and in addition the solvents can be slowly evaporated at room temperature. The sedimentary colloidal crystal grains were obtained by drying the colloidal silica spheres dispersion in small flasks. Due to the volatile nature of the solvents, they slowly evaporated from the flasks over the course of several months or years. During this time the particle concentration slowly increased and crystals were formed, followed by full drying of the sediments. Crystalline sediments could be identified by the presence of strong Bragg reflections.

2.2.3 Fiber Preparation

Carbon fibers of 10 μm thick were provided by J. Gulden from Hasylab at DESY in Hamburg, Germany. The fibers were cut to a length of 5 mm using a razor blade and connected to glass sample pins of 2 mm in diameter using Bison Epoxy glue[®]. The glass pins were inserted into a magnetic adjustable crystal mount (Hampton Research) that can be placed on a goniometer head.

Colloidal crystal grains of various sizes were obtained by manual crushing a piece of the ordered sediments or by scraping a convective colloidal crystal film

with a razor blade. Small individual grains of approximately 5 μm were identified using a Leica M205 C Stereomicroscope having the advantage of a large working distance ($\sim 5\text{ cm}$) at high ($800\times$) magnification. The selected grains were picked up manually using a micromanipulator (PatchMan NP2, Eppendorf) and connected to the tip of a carbon fiber. The connection to the fiber was either caused by attractive electrostatic forces or by dipping the fiber into a very small amount of one of the components of Bison Epoxy glue[®] with the micromanipulator, this results in a sticky fiber surface but prevents the formation of glue drops that complicates crystal grain pick-up.

2.2.4 Characterization of Colloidal Crystals

The structure and thickness of the colloidal crystal films and grains were studied with scanning electron microscopy (SEM) with a Phenom G2 desktop SEM and Philips XLFE30. SEM samples were prepared by breaking the substrate into smaller pieces (if necessary) that were connected to SEM stubs with conductive carbon tape, scratched with a razor blade to reveal their inner structure and sputter-coated with 6 nm platinum. Fibers with colloidal crystal grains were either connected to the SEM stubs via their glass pins with carbon tape or removed from the glass pins and placed onto the stub directly. Focused ion beam (FIB) lithography was performed with a FEI Nova Nanolab 600 Dual beam apparatus, which uses Gallium ions to cut through structures.

2.3 Results

2.3.1 Colloidal Crystal Films Prepared via Vertical Deposition

Colloidal crystal films of different particle composition, size and layer thickness were needed for different X-ray diffraction studies. Therefore, many different colloidal crystal films were prepared with the vertical deposition method. For the repeated fabrication of a large number of colloidal crystal films readily available materials were used that consisted of thin glass microscope slides as substrates and scintillation vials of 20 mL as dispersion containers. Other experimental control parameters, such as substrate angle, dispersion solvent and oven temperature were also optimized. Slides of $40 \times 12.5\text{ mm}$ in size were used because these fit into the scintillation vials easily and provide a substrate angle of $\sim 30^\circ$. Due to the angle, a colloidal crystal film is only formed on the front side of the substrate. The best solvents were found to be water for polystyrene particles and ethanol for silica particles that should be evaporated around 50–55 $^\circ\text{C}$ and 65–70 $^\circ\text{C}$, respectively.

By using the optimal experimental conditions during the vertical deposition it was possible to produce colloidal crystal films that fully covered the substrate and that showed the presence of large single crystal regions. Figure 2.1a shows photographs of typical colloidal crystal films of differently sized polystyrene and silica spheres that were prepared. Under white illumination these films show distinct Bragg reflections with different colors depending on particle size indicating the presence of ordered structures. The vertical stripes are the result of twinning crystal structures. Homogeneous full substrate covering films were obtained for all differently sized polystyrene particles and for silica particles with $R < 150$ nm. Figure 2.1a–c show three typical films obtained for BvR_I3, PS1 and DB275. However, for larger silica particle sizes, the films were usually found to be inhomogeneous. Due to the relatively fast sedimentation of the particles, their flux towards the meniscus decreases over time. For TPM coated silica particles DB360 with $R = 246$ nm a typical film is shown in Fig. 2.1d, where a large uncovered part is present in the middle part and the thickness of the film clearly decreases towards the bottom of the substrate. For all colloidal crystal films the thickness was found to become less homogeneous towards the bottom part of the substrate. This is caused by a change in meniscus shape at this solvent height induced by the close proximity of the bottom and walls of the scintillation flasks changing the meniscus shape and thus the particle influx.

SEM measurements showed that the colloidal spheres crystallized into a face centered cubic (FCC) structures, with the (111) face parallel to the glass substrate as expected [14]. Figure 2.2 shows the SEM images of colloidal crystal films of polystyrene particles PS1. The films contains large cracks that run from top to bottom (Fig. 2.2a), this is a commonly observed drying effect caused by tensile stresses during solvent evaporation decreasing the distance between the particles. In the SEM images additional shrinkage is caused by the exposure to electrons and the high vacuum in the SEM [15]. Depending on the number of layers the distance between the cracks changes. For films of polystyrene particles consisting of only a few layers the cracks are much smaller. Films prepared from silica particles showed less cracks, because these particles shrink less in size than the polystyrene particles

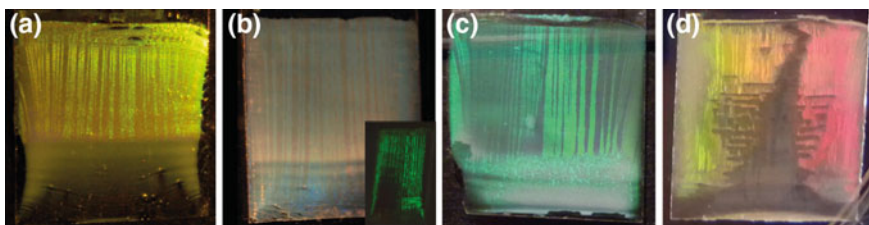


Fig. 2.1 Photographs of colloidal crystal films of 10×10 mm prepared from a 5 mL suspension of **a** 0.25 vol% BvR_I3 particles in water with $R = 136$ nm dried at 50°C . **b** 0.25 vol% PS1 particles in water with $R = 208$ nm dried at 55°C , *inset* shows the film with a different orientation resulting in *strong green* Bragg reflections. **c** 1.0 vol% DB275 particles in ethanol with $R = 118$ nm dried at 60°C and **d** 0.5 vol% DB360 particles in ethanol with $R = 246$ nm dried at 70°C

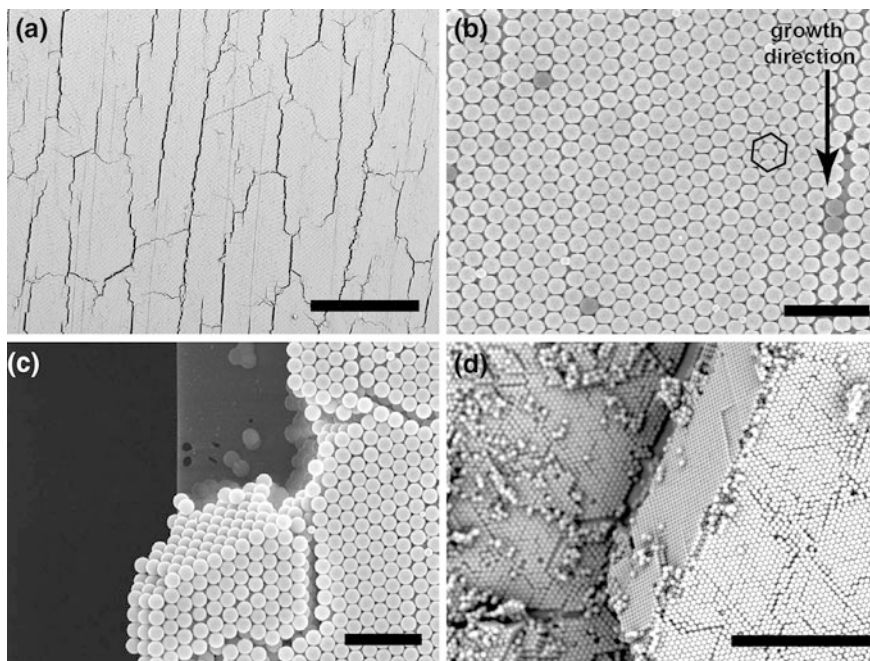


Fig. 2.2 SEM images of a colloidal crystal film of polystyrene particles PSI. **a** Overview of large area that shows *drying cracks*. **b** A higher magnification of the colloidal crystal film *top layer* where the particles are ordered in a *hexagonal arrangement*. **c** The edge of a crystal consisting of 9 layers and **d** a scratched region of a crystal with >30 layers. Scale bars are **a** 50 μm , **b**, **c** 2 μm and **d** 10 μm

upon solvent evaporation. Furthermore, it has been shown for silica particles that sintering at high temperatures can prevent the crack formation.

Figure 2.2b shows the top layer of the crystal, where the hexagonal arrangement of the spheres in the layers can be clearly seen as indicated by the hexagon. The orientation of the hexagonal order in the layers was consistently found to be aligned within $\sim 15^\circ$ along the growth direction as indicated by the arrow. Why this orientation is obtained is not clear but could be related to the growth process that involves several transitions in layer thickness at the start and is furthermore influenced by the solvent flux. For more details on the growth process see Ref. [16–18].

The SEM measurements also provide insight into the layer thickness of the crystals. By scraping the crystal with a razor blade the inner structure of the crystal and the number of layers could be estimated. As expected the thickness of the films was controlled by the particle concentration if all other conditions were kept constant. Figure 2.2c shows a crystal of polystyrene spheres consisting of nine layers while Fig. 2.2d shows a crystal where at least thirty layers can be distinguished. The number of layers was found to increase rapidly at the start of the film followed by a region with an almost constant number of layers. The films increased only with a few layers over a range of a few mm. At the end of the films the thickness was

usually found to increase rapidly and the structure became disordered. This is caused by a higher particle flux as a result of the increase of the particle concentration caused by the solvent evaporation and the change in meniscus shape, as discussed previously.

The growth process was also performed on different substrates, such as silicon wafers coated with silicon nitride (Si_3N_4) membranes of different thickness and size. Because the wetting of Si_3N_4 is very different from that of SiO_2 the VD conditions had to be optimized for these studies. For Si wafers of 23×23 mm with an array of windows sized 250×250 μm the optimal conditions were a 0.1 vol% dispersion of polystyrene spheres in ethanol placed into scintillation vial of which the screw top was removed and dried at 25 °C over several days.

2.3.2 Single Colloidal Crystals Grains on a Fiber Tip

For CXDI measurements one of the requirements is that the colloidal crystal grains should be much smaller than the coherence length of the X-ray beam to ensure coherent irradiation. For the experiment described below the goal was to have a grain size around 5 μm . Colloidal crystals obtained via sedimentation or vertical deposition were used as source for the grains.

The sedimentary crystals were prepared by slow settling of silica particle dispersions. Figure 2.3a shows the crystallization of the TPM coated silica particles DB239 upon sedimentation in ethanol/toluene mixture. Clear Bragg reflections can be seen from the top of the sediment indicating the presence of crystals. After drying the obtained colloidal crystal sediments were manually broken into smaller pieces and the crystal quality was checked. Figure 2.3b shows the surface of a small crystal grain consisting of DB284 particles imaged with light microscopy that shows the presence of different orientated grains, indicated by the Bragg reflection of different colors, as expected for a sedimentary crystal. SEM measurements revealed the presence of a large number of ordered layers in the colloidal crystal

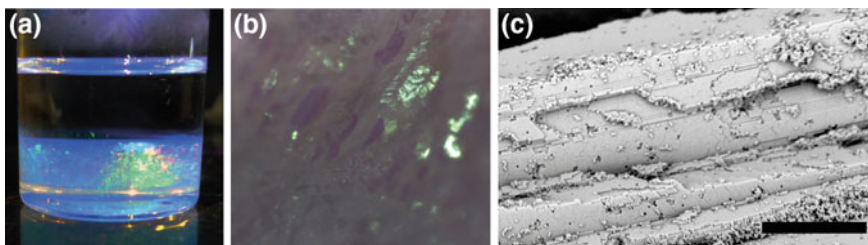


Fig. 2.3 **a** Photograph of the sedimentation of TPM coated silica spheres DB239 in an ethanol toluene mixture. **b** Light microscopy image of the surface of a large colloidal crystal grain of stearyl coated silica spheres DB284 obtained after drying and breaking of an ordered sediment and **c** SEM image of the edge of a colloidal crystal grain of DB359 spheres. Scale bar is 10 μm

grains. Figure 2.3c shows the surface of a large grain consisting of DB359 particles where the layers can be clearly distinguished. The rough edges, particle clusters and vacancies indicate that the mechanical crushing does damage the crystals slightly but the overall order is retained, making them suitable candidates for the preparation of small colloidal crystal grains.

With the vertical deposition method colloidal crystal films were prepared from silica and polystyrene particles as described in Sect. 2.3. To obtain colloidal crystal grains the films were scratched with a razor blade. Figure 2.4 shows the effect of scratching on the crystals made from polystyrene spheres and TPM coated silica spheres. The crystal of silica spheres is destroyed close to the scratch and a random structure of spheres is left behind. The crystal of polystyrene spheres shows the presence of small chunks of crystals that have come loose off the glass substrate. This difference in behavior can be explained by a difference in interaction between the particles and between the particles and the substrate. The silica particles are in contact through their TPM coating layers that apparently deform easily. While the polystyrene particles seem to have formed strong bonds and the crystals break along the drying cracks which preserves the crystal order. Therefore, the colloidal crystal films of polystyrene spheres were used as source for their grains. With the additional advantage that the crystal grain thickness can be controlled with the initial particle concentration in the VD experiment.

The next step was selecting the grains with a proper size of $\sim 5 \mu\text{m}$ and connecting these to the tip of a carbon fiber. The grains were obtained by manually smashing macroscopically large colloidal crystal grains. As this is not a controlled process and the larger grains are likely to break at the points of least resistance, a collection of grain sizes is obtained. Figure 2.5a shows a microscopy image obtained at the highest magnification ($800\times$) of the stereo microscope where the arrows indicate a few grains of suitable size. The inset shows the full overview of all different grain sizes that are present. It is impossible to determine in this step whether the grains have retained their crystalline order. However, the crystal quality of the obtained crystal grains from the bulk sediments was checked with the SEM.

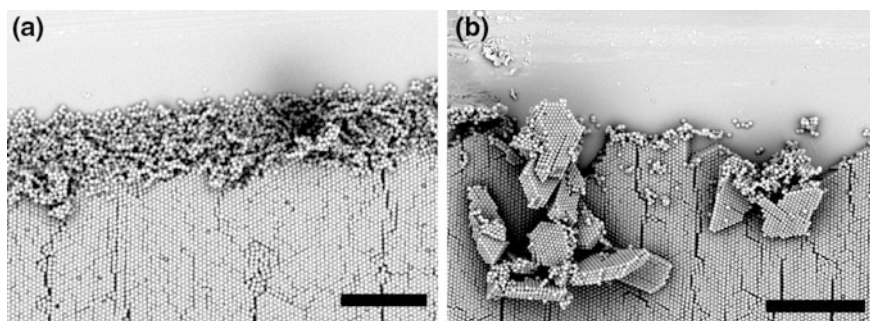


Fig. 2.4 SEM image of colloidal crystal film close to a scratch of **a** silica particles DB360 coated with TPM and **b** polystyrene particles PSI. Scale bars are $10 \mu\text{m}$

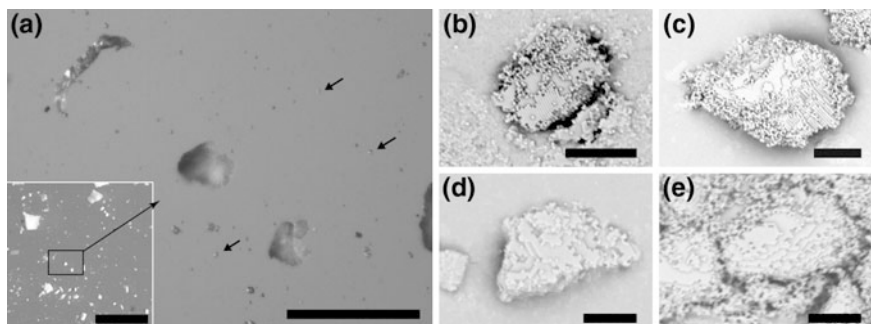


Fig. 2.5 **a** Stereo microscopy image at highest magnification of variously sized colloidal crystal grains of particles DB359, grains of $\sim 5 \mu\text{m}$ are indicated with the *arrows* (*inset*) low magnification image showing the large deviation in grain sizes obtained after crushing, **b–d** SEM image of a small colloidal crystal grains consisting of; **b** DB359 **c** DB284 **d–e** DB275. In most grains the ordered layers can be observed indicating the order is preserved during crushing for these silica particles. Scale bars are **a** $200 \mu\text{m}$ (*inset* 1 mm), **b–e** $5 \mu\text{m}$

Figure 2.5b–e shows a few examples of crystalline grains obtained from several different silica particles. The grains show the presence of a number of differently sized layers. Besides these crystalline grains it is clear that also amorphous structures are present. One can therefore never be sure if the picked up grain is truly a colloidal crystal grain.

After selection of a properly sized grain, it was connected to a carbon fiber by bringing the fiber in close contact with the grain by use of a micromanipulator. The connection was made via either electrostatic forces or using (a single component of) epoxy glue. The first will not produce background during the CXDI measurement but has a low success rate, while the latter will increase the background and might even destroy the grain but provides a very stable bond. Figure 2.6a shows an example of a colloidal crystal grain on a fiber tip after successful pickup. A SEM

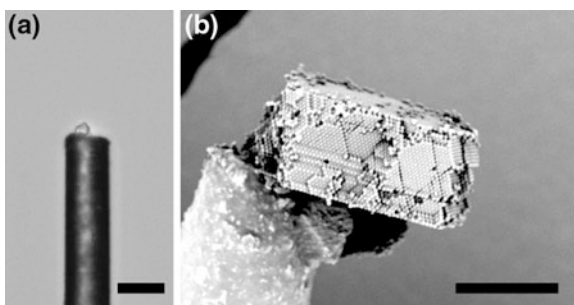


Fig. 2.6 **a** Microscopy image of a colloidal crystal grain on a carbon fiber tip. **b** SEM image of a colloidal crystal grain of polystyrene particles attached by glue to the fiber tip after pickup. Scale bars are **a**, **b** $10 \mu\text{m}$

image of a polystyrene sphere crystal grain picked up with glue is shown in Fig. 2.6b. For the electrostatic connected grains SEM imaging is impossible as the additional charging by the electrons destroys the bond between grain and fiber. The SEM image shows that the crystalline order is still present and several different layers can be distinguished. The SEM analysis also showed that the selection does not always result in grains of proper size.

CXDI experiments were performed with a large number of the picked up colloidal crystal grains. These measurements showed that many conditions have to be right for a successful CXDI experiment. It turned out that from all prepared crystals on a fiber (>200 samples) only two or three crystal grains produced scattering data of proper quality. There were several reasons for this low success rate. First of all, the measurements showed that the colloidal crystals were easily removed from the fibers. Secondly, not all of the selected grains were found to be crystalline. Thirdly, silica particles produced much better signals than polystyrene particles of the same size. The higher electron density of silica provides a much better X-ray contrast and hence signal-to-noise ratio than the polystyrene spheres. Although SEM measurements showed the polystyrene crystals always retain their crystal order upon breaking, even very large crystal grains (>20 μm) did not provide a proper signal. However, when a properly connected colloidal crystal grain consisting of silica particles that retained its crystal structure was imaged, high quality scattering data could be obtained over a full 180° rotation.

2.4 Conclusions and Outlook

The vertical deposition method was applied successfully for the preparation of colloidal crystal films of polystyrene and silica particles. By tuning the experimental vertical deposition parameters, the crystal growth process was controlled and the desired thickness and surface covering on different substrates was achieved. The obtained crystals display a similar crystal orientation and thickness over a large sample area and makes them very suitable for X-ray diffraction studies.

Two different kinds of synchrotron X-ray diffraction studies were performed of the colloidal crystal films. A pump-probe study of the effect of strong optical fields on the colloidal crystal and the particle dynamics was performed and is described in Sect. 2.5.1. Also a microradian X-ray diffraction ($\mu\text{rad-XRD}$) study was performed to clarify the effect of temperature on the structure and bulk properties of the colloidal crystals and is described in Sect. 2.5.2.

For CXDI measurements colloidal crystal grains are needed and it was shown that the most suitable particles are coated silica spheres. The colloidal crystals of the silica spheres should be prepared via slow sedimentation followed by drying because the grains produced from these sediments retain their crystalline order upon sediment fracture, in contrast to convective-assembly crystals. In addition, the high X-ray contrast of the silica resulted in the strongest CDXI signals.

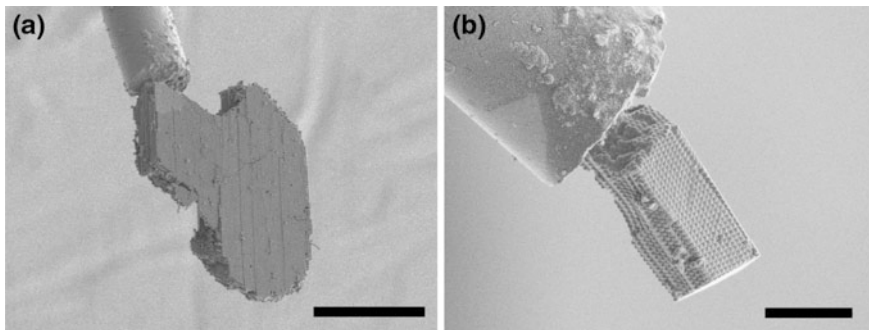


Fig. 2.7 SEM images of the FIB cutting process of sizing down **a** a large colloidal crystal grain of polystyrene spheres to **b** a size of $5 \times 10 \mu\text{m}$. Scale bars are **a** $20 \mu\text{m}$ and **b** $5 \mu\text{m}$

In the future, the process of crystal grain selection could be improved. Now the grain selection results in grains of improper size and/or non-crystallinity. A way to improve the selection is employing Focused Ion Beam (FIB) processing. With this method colloidal crystal grains could be cut to any desired size. Preliminary experiments showed that this can indeed be achieved. Figure 2.7 shows the sizing down procedure of a large crystal grain of polystyrene spheres (Fig. 2.7a) milled down to a smaller size (Fig. 2.7b). Clearly, the FIB technique is a very suitable technique for the preparation of properly sized crystal grains. In addition, the in situ SEM imaging provides direct information about the crystal quality and makes the search for proper colloidal crystal grains easier.

2.5 X-ray Diffraction Experiments of Colloidal Crystals of Spheres

2.5.1 Pump-Probe Experiments with Free Electron Lasers

The colloidal crystal films of polystyrene spheres described in Sect. 2.3 were used for several studies. In this section a short description is given of the experiment and results of pump-probe experiments of these films as reported by Dronyak et al. [19].

The self-assembled colloidal crystal films of polystyrene films are of interest for the bottom-up fabrication [20] of a new class of nano-materials, such as hypersonic phononic crystals [21]. It has been shown that colloidal crystals of polystyrene spheres can possess a phononic band gap in the gigahertz frequency range [22]. To characterize and understand these properties the ultrafast dynamics in the colloidal crystal were studied with an advanced free-electron laser (FEL). Time-resolved experiments of the temporal changes in the sample induced by infrared (IR) laser pulses of 800 nm and imaged with soft X-rays with a wavelength of 8 nm (154.98 eV) at the BL3 beamline were performed at FLASH. Figure 2.8 shows a

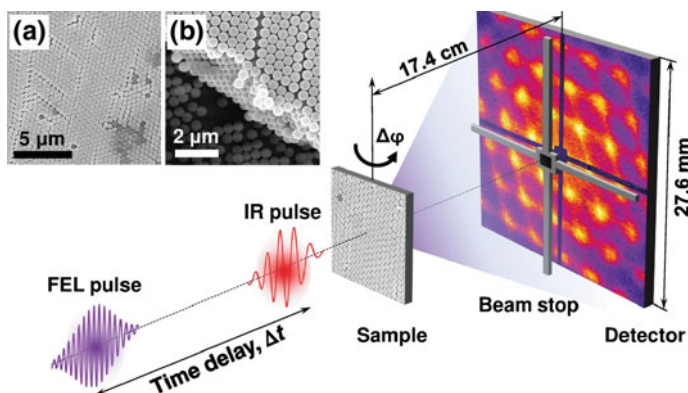


Fig. 2.8 Schematic view of the pump-probe experiment showing the IR pump (IR pulse) and the soft X-ray probe (FEL pulse) separated by a time delay Δt , the sample, and the detector, which is protected by the beam stop. *Insets a and b* show SEM images of the colloidal crystal film used in the experiment. The 11 layers of polystyrene spheres composing the colloidal crystal are visible in the *inset (b)*. Reproduced with kind permission from Ref. [18]. Copyright 2013 American Physical Society

schematic representation of the performed experiment. A single IR pulses was used to pump the sample, followed by a single FEL pulse with a time delay, Δt , to probe the instantaneous structure. The time delay could be controlled with picosecond resolution and time delays of -100 to $+1000$ ps were used. The sample was a colloidal crystal film consisting of polystyrene particles on a Si_3N_4 membrane of 100 nm thick. The diffraction patterns produced by the transmitted FEL beam were collected by a detector at 17.4 cm behind the sample.

Analysis of the Bragg peak position, intensity and shape was performed to reveal the effect of the IR pulse on the crystal and the colloidal spheres. Fourier transforms of the time dependent parameters was used to determine the characteristic frequencies. This showed that an increased contribution was present in the frequency region of 4–5 GHz. Comparing this result to the Lamb theory showed that the breathing mode of the polystyrene spheres was probed in the experiments.

A follow-up experiment was performed in April 2014 at the Linac Coherent Light Source (LCLS), at SLAC in Stanford, USA, together with the Hamburg team headed by Prof. Ivan Vartanyants. The results are currently being analyzed.

2.5.2 *In Situ Structural Evolution upon Heating with X-ray Diffraction*

Another study that was performed of the colloidal crystal films of polystyrene films was focused on the structural evolution of the crystal upon heating as reported by Zozulya et al. [23]. This study focused on the changes in the colloidal crystals upon

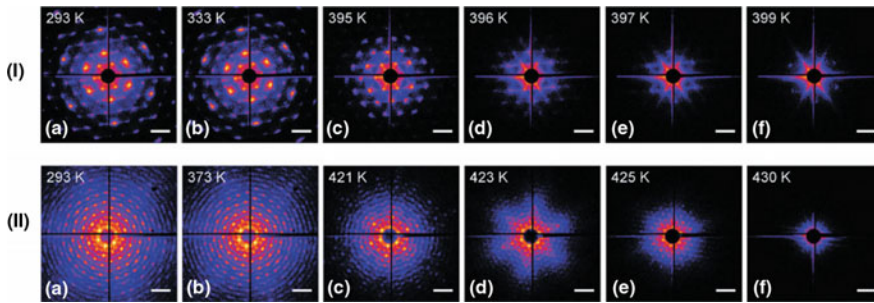


Fig. 2.9 In situ diffraction patterns of colloidal crystals consisting of polystyrene spheres PS2 with $R = 82$ nm (*top row*) and PS1 with $R = 208$ nm (*bottom row*) measured during incremental heating. The sample temperature is marked at the *top left* corner for each of the displayed patterns. This image is taken from Ref. [22]. Reproduced with permission of the International Union of Crystallography

heating, as it has been shown that with elevated temperatures the photonic properties of a colloidal crystal film can be modified [24–26]. Furthermore, the particle size, which increases the surface-to-volume ratio, will affect the glass transition temperature of polystyrene [27–29]. Understanding both effects is important for the potential use of the polystyrene crystals as photonic materials. For the in situ investigation of the effect of temperature, X-ray diffraction is very well suited due to the high penetration depth and nondestructive characterization approach.

The experiment was performed at the P10 coherence beamline of the PETRAIII synchrotron facility at DESY, Hamburg. Colloidal crystal films prepared on glass microscope slides from two differently sized linear polystyrene spheres, PS2 $R = 82$ nm and PS1 $R = 208$ nm, were used. The films were slowly heated with small temperature steps over a range of 293–430 K. Diffraction patterns were measured with a photon energy of 15 keV and were collected by a detector located 5.2 m behind the sample.

Figure 2.9 shows the diffraction patterns of the colloidal crystal films consisting of the two differently sized polystyrene particles. Upon a temperature rise the deterioration and disappearance of the higher order Bragg peaks was observed, followed by enhancement of the diffuse scattering with hexagonal symmetry. This indicated that the polystyrene particles first slowly deformed into a dodecahedron shape before completely melting. The crystal lattice was also found to shrink slightly upon heating and finally completely disappeared.

From the total scattered intensity the glass transition temperature was determined to be 30 K lower for the smaller particle PS2 than the larger particles PS1. This showed that the glass transition temperature of the polystyrene is strongly affected by the particle size and hence the surface-to-volume ratio.

Acknowledgments This work is the result of the many collaborations with the group of Ivan Vartanyants from HasyLab and Alexey Zozulya and Michael Sprung of the P10 beamline staff of PETRAIII, both located at DESY in Hamburg, Germany. Johannes Gulden, Anatoly Shabalin,

Roman Dronyak, Ruslan Kurta, Oleksandr Yefanov, Dmitry Dzighaev, Oleg Gorobstov, Andrej Singer and Ulf Lorenz are thanked for their help during the X-ray measurements. Jan Hilhorst is acknowledged for his help with the initial vertical deposition experiments. Bas van Ravensteijn and Daniela Kraft are thanked for kindly providing two of the polystyrene particles. Matthijs de Winter is thanked for performing the FIB experiments.

References

1. J.F. Galisteo-Lopez, M. Ibisate, R. Sapienza, L.S. Froufe-Perez, A. Blanco, C. Lopez, *Adv. Mater.* **23**, 30–69 (2011)
2. A.C. Blanco, E.S. Grabtchak, M. Ibisate, S. John, S. Leonard, C. Lopez, F. Meseguer, H. Miguez, J. Mondia, G. Ozin, O. Toader, H.M. van Driel, *Nature* **405**, 437–440 (2000)
3. Y. Vlasov, X.Z. Bo, J.C. Sturm, D.J. Norris, *Nature* **414**, 289–293 (2001)
4. A. Bosak, I. Snigireva, K.S. Napolskii, A. Snigirev, *Adv. Mater.* **22**, 3256–3259 (2010)
5. J. Hilhorst, M.M. van Schooneveld, J. Wang, E. de Smit, T. Tylicszczak, J. Raabe, A.P. Hitchcock, M. Obst, F.M.F. de Groot, A.V. Petukhov, *Langmuir* **28**, 3614–3620 (2012)
6. D.V. Byelov, J.M. Meijer, I. Snigireva, A. Snigirev, L. Rossi, E. van den Pol, A. Kuijk, A. Philipse, A. Imhof, A. van Blaaderen, G.J. Vroege, A.V. Petukhov, *RCS Advances* **3**, 15670–15677 (2013)
7. J. Gulden, O.M. Yefanov, A.P. Mancuso, V.V. Abramova, J. Hilhorst, D. Byelov, I. Snigireva, A. Snigirev, A.V. Petukhov, I.A. Vartanyants, *Phys. Rev. B* **81**, 224105 (2010)
8. J. Gulden, O.M. Yefanov, A.P. Mancuso, R. Dronyak, A. Singer, V. Bernatova, A. Burkhardt, O. Polozhentsev, A. Soldatov, M. Sprung, I.A. Vartanyants, *Opt. Express* **20**, 4039–4049 (2012)
9. J.R. Fienup, *Appl. Opt.* **21**, 2758–2769 (1982)
10. V. Elser, *JOSA A* **20**, 40–55 (2003)
11. K.A. Nugent, *Adv. Phys.* **59**, 1–99 (2010)
12. A.P. Philipse, A. Vrij, *J. Colloid Interface Sci.* **128**, 121–126 (1989)
13. A.K. Van Helden, J.W. Jansen, A. Vrij, *J. Colloid Interface Sci.* **81**, 354–368 (1981)
14. P. Jiang, J.F. Bertone, K.S. Hwang, V.L. Colvin, *Chem. Mater.* **11**, 2132–2140 (1999)
15. N. Denkov, O. Velev, P. Kralchevski, I. Ivanov, H. Yoshimura, K. Nagayama, *Langmuir* **8**, 3183–3190 (1992)
16. L. Meng, H. Wei, A. Nagel, B.J. Wiley, L.E. Scriven, D.J. Norris, *Nano Lett.* **6**, 2249–2253 (2006)
17. D.D. Brewer, J. Allen, M.R. Miller, J.M.D. Santos, S. Kumar, D.J. Norris, M. Tsapatsis, L.E. Scriven, *Langmuir* **24**, 13683–13693 (2008)
18. D.J. Norris, E.G. Arlinghaus, L. Meng, R. Heiny, L.E. Scriven, *Adv. Mater.* **16**, 1393–1399 (2004)
19. R. Dronyak, J. Gulden, O.M. Yefanov, A. Singer, T. Gorniak, T. Senkbeil, J.M. Meijer et al., *Phys. Rev. B* **86**, 064303 (2012)
20. F. Marlow, P. Sharifi, R. Brinkmann, C. Mendive, *Angew. Chem.* **48**, 6212–6233 (2009)
21. T. Gorishnyy, C. Ullal, M. Maldovan, G. Fytas, E. Thomas, *Phys. Rev. Lett.* **94**, 115501 (2005)
22. W. Cheng, J. Wang, U. Jonas, G. Fytas, N. Stefanou, *Nat. Mater.* **5**, 830–836 (2006)
23. A.V. Zozulya, J.M. Meijer, A. Shabalin, A. Ricci, F. Westermeier, R.P. Kurta, U. Lorenz, A. Singer, O. Yefanov, A.V. Petukhov, M. Sprung, I.A. Vartanyants, *J. Appl. Cryst.* **46**, 903–907 (2013)
24. H. Miguez, F. Meseguer, C. Lopez, A. Blanco, J.S. Moya, J. Requena, A. Mifsud, V. Fornes, *Adv. Mater.* **10**, 480–483 (1998)

25. B. Gates, S.H. Park, Y.N. Xia, *Adv. Mater.* **12**, 653–656 (2000)
26. T. Deng, J. Zhang, K. Zhu, Q. Zhang, J. Wu, *Mater. Chem. Phys.* **129**, 540–546 (2011)
27. J.L. Keddie, R.A.L. Jones, R.A. Cory, *Europhys. Lett.* **27**, 59–64 (1994)
28. J.A. Forrest, K. Dalnoki Veress, J.R. Stevens, J.R. Dutcher, *Phys. Rev. Lett.* **77**, 2002–2005 (1996)
29. O. Baeumchen, J.D. McGraw, J.A. Forrest, K. Dalnoki-Veress, *Phys. Rev. Lett.* **109**, 055701 (2012)

<http://www.springer.com/978-3-319-14808-3>

Colloidal Crystals of Spheres and Cubes in Real and
Reciprocal Space

Meijer, J.-M.

2015, XIV, 155 p. 84 illus., 28 illus. in color., Hardcover

ISBN: 978-3-319-14808-3